It appears, see Fig. 1 and 2, that more chemical reactions, deposition and or precipitation of corrosion products occurred in sulfur-rich melts, *i.e.*, Na_2S_5 and pure sulfur, and that more dissolution of corrosion products occurred in sulfur-poor melt, *i.e.*, Na_2S_2. This is perhaps due to the changes of the solubility of the sulfates in the sulfide melts as the composition of the sulfides changes.

Conclusions

Sodium β"-alumina electrolytes are chemically attacked by Na_2S_x melts and pure sulfur during immersion at high temperatures. The likely reactions can be written as described in Eq. [4.1]-[4.7], and occur preferentially on surface imperfections of the solid electrolyte.

The thermodynamically stable corrosion products are Na_2SO_4, $NaAl(SO_4)_2$, $Al_2(SO_4)_3$, $NaHSO_4$, Na_2CO_3, and NaOH. Most of these have high melting point and deposit on the electrolyte surface. Some have a low melting point and can be dissolved in the polysulfide melts, leading to dissolution or etching of the electrolyte surface.

There is a limited solubility of sodium sulfates in sodium sulfide melts. Precipitation of the crystallized sulfates occurred after prolonged exposure to sulfide melts and occurred preferentially at imperfections such as boundaries of large grains, or surface steps on the electorlyte surface.

The degree of corrosion increased as the content of sulfur increased in the range of Na_2S_2 to Na_2S_5 to sulfur.

In addition to the reactions between the electrolyte and Na_2S_x or sulfur, the corrosion products of transition metals, and current collector material (graphite), also deposit on the electrolyte surface.

All of the corrosion reactions were greatly accelerated by contaminations of impurities, such as water and oxygen, and transition metals.

In a practical cell, the environment that the electrolyte will be exposed to is expected to be a combination of the above situations to some degree. The degraded layer formed on electrolyte surfaces in an actual Na/S cell would be expected to be a mixture of (*i*) sulfates and carbonates, produced by reactions [4.1] through [4.6], and (*ii*) corrosion products of cell parts, by reactions [4.7]. This layer may block sodium-ion transport, cause inhomogeneous current distribution, and could spall off when new compounds form underneath it, leading to a progressive degradation of positive electrode contact interface of the electrolytes.

Since the corrosive power of the polysulfide melts increases at a composition corresponding to the fully charged state and is enhanced for free sulfur, it would seem advisable to avoid heterogeneous electrode reactions that expose the electrolyte surface for unnecessarily long periods to the most corrosive sulfide melts that may occur at the end of charge.

Acknowledgments

The authors wish to thank Dr. S. Visco for valuable discussions and suggestions. This work was supported by the U.S. Department of Energy under contract no. DE-AC03-76SF00098.

Manuscript submitted July 7, 1986; revised manuscript received Aug. 12, 1987.

Lawrence Berkeley Laboratory assisted in meeting the publication costs of this article.

REFERENCES

1. L. C. De Jonghe, L. Feldman, and A. Buechele, *Solid State Ion.*, **5**, 267 (1981).
2. L. C. De Jonghe, L. Feldman, and A. Buechele, *J. Mater. Sci.*, **16**, 780 (1981).
3. N. S. Choudhury, *This Journal*, **133**, 425 (1986).
4. M. L. Miller, B. J. McEntire, G. R. Miller, and R. S. Gordon, *Am. Ceram. Soc. Bull.*, **58** (5), 522 (1979).
5. R. N. Singh, *ibid.*, **67** (10), 637 (1984).
6. J. T. Kummer, "Progress in Solid State Chemistry," Vol. 7, H. Reiss and J. O. McCaldin, Editors, pp. 141-175, Pergamon Press, Inc., New York (1972).
7. M. Itoh, K. Kimura, and Z. Kozuka, *Trans. Jpn. Inst. Met.*, **26**, 353 (1985).
8. N. K. Gupta and R. P. Tischer, *This Journal*, **119**, 1033 (1972).
9. The NBS Tables of Chemical Thermodynamic Properties, *J. Phys. Chem. Ref. Data*, **11**, Suppl. no. 2 (1982).
10. "JANAF Thermochemical Tables," 2nd ed., U.S. Department of Commerce, National Bureau of Standards, Vol. 37, (1971, 1978); *J. Phys. Chem. Ref. Data*, **11** (3) (1982).
11. D.-S. Park, Proceedings of DOE/EPRI Beta (Sodium-Sulfur) Battery Workshop V, EPRI EM-3631-SR, pp. 6-191 (1984).
12. J. E. Battles, Proceedings of DOE/EPRI Beta (Sodium-Sulfur) Battery Workshop V, EPRI EM-3631-SR, pp. 6-291 (1984).

Development of Low Chromium Substitute Alloys for High Temperature Applications

Je M. Oh*

United States Department of the Interior, Bureau of Mines, Albany Research Center, Albany, Oregon 97321

ABSTRACT

The oxidation of a base-line Fe-8Cr-16Ni (weight percent) composition was compared to that of alloys with small additions of Al, Si, Mo, and Mn. Oxidation was done in air over the temperature range of 600°-1000°C for up to 1000h. Alloys that contained Al and Si showed excellent oxidation resistance because of the formation of a layer containing Si at the scale-metal interface. Small additions of Al seemed to form oxide nuclei during a transient oxidation period, aided the formation of a layer containing Si and/or a chromium oxide, and provided better oxide adherence. Molybdenum and manganese additions stabilized a fully austenitic microstructure at room temperature. The oxidation behavior of these alloys was compared to that of 304 stainless steel and some commercial superalloys. Reaction kinetics, oxide morphologies, and oxidation mechanisms of the substitute alloys are described.

One of the Bureau of Mines research goals is to minimize the requirement for domestically scarce minerals through substitution and conservation. Chromium, in particular, is the element which provides the characteristics of oxidation and corrosion resistance to stainless steels (SS) by forming a protective chromium oxide scale. Because the United States has no commercial chromium deposits, chromium is considered to be a particularly vulnerable strategic metal. Therefore, there is interest in developing low chromium alloys that could substitute for stainless steels in some applications. A significant fraction of the stainless steel used in the United States is used in applications where resistance to high temperature oxidation is important.

*Electrochemical Society Active Member.

Table I. Alloy compositions

Alloy	Fe	Cr	Ni	Si	Al	Mo	Mn	Co	W
A	Bal	7.9	16						
B	Bal	7.9	16.1	3.3					
C	Bal	8	15.9	3.35	0.96				
D	Bal	7.9	16	3.37	0.95	1.96			
E	Bal	8	16	3.32	0.97	1.95	0.91		
304 SS	Bal	18	8	0.5		0.3	1.0		
Hastelloy C-276	5	15	Bal			16	0.8	2.5	4
Incoloy 800	46	21	32.5	0.5	0.38		0.75		
Inconel 600	8	15.5	Bal	0.25	0.3		0.5		

To lower the chromium content yet maintain oxidation resistance similar to that of stainless steels, an alloy should contain at least one element whose oxide offers protection equivalent to that of chromium oxide. Aluminum and silicon are the two most common and inexpensive elements whose oxides form stable and protective scales. Therefore, most of the alloys being considered as possible stainless steel substitutes, with or without Cr, contain additions of at least one of these elements (1-4).

Some research has been done for stainless steels containing 9-12% Cr (5-6). In this study, individual alloying elements were systematically added to a low Cr stainless steel with a nominal composition of Fe-8Cr-16Ni to evaluate the effect of alloying elements on their high temperature oxidation kinetics and the oxide morphology so that an optimum alloy composition can be determined.

Experimental

Alloys were prepared from electrolytic grades of Fe, Cr, Ni, Si, Al, Mo, and Mn. These materials were arc melted into buttons (100g) in an argon atmosphere. The buttons were homogenized in vacuum for 24h at 1200°C and then hot-rolled at 1050°C with 20% reduction of thickness per pass. Coupons were cut from the rolled buttons, polished down to 600 grit, ultrasonically cleaned, and degreased with alcohol and acetone.

A Cahn RG electrobalance was used to obtain short-term kinetic data. For long-term (more than 100h) experiments, specimens were hung on a quartz rack and oxidized up to 1000h in static air. After thermal cycling to room temperature, the weight change was measured using an analytical balance with an accuracy of ±0.1 mg. Detailed thermal cycling frequencies are presented in the following section.

The oxidized specimens were examined using scanning electron microscopy (SEM), energy dispersive x-ray analysis (EDXA), x-ray diffraction, and optical microscopy. Some specimens were mounted in epoxy and cross-sectioned to obtain elemental profiles. The alloy compositions are tabulated in Table I.

Results

Thermogravimetric data.—The short-term specimens were oxidized in air for 24h at 600°C. However, with the ex-

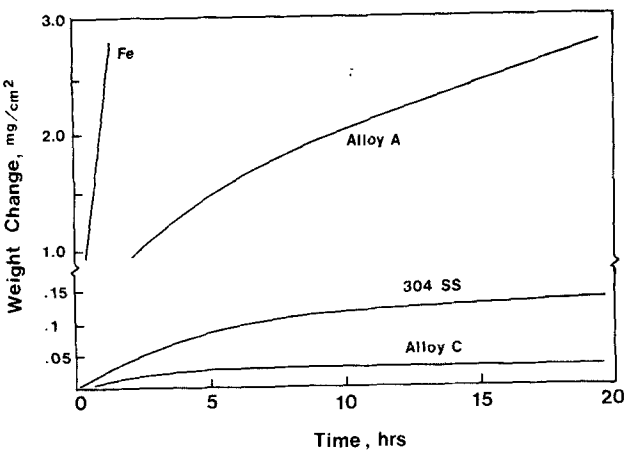

Fig. 1. Reaction kinetics of alloys at 750°C

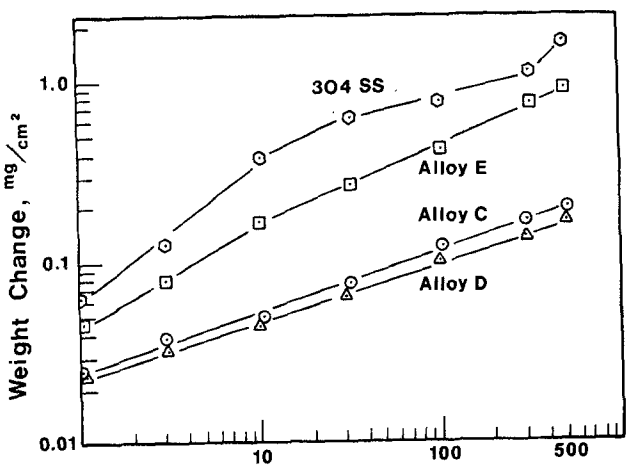

Fig. 2. Reaction kinetics of alloys at 900°C

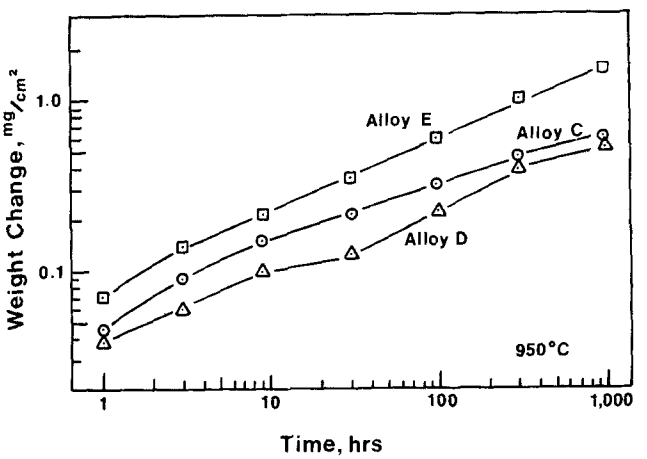

Fig. 3. Reaction kinetics of alloys on a log-log scale at 950°C

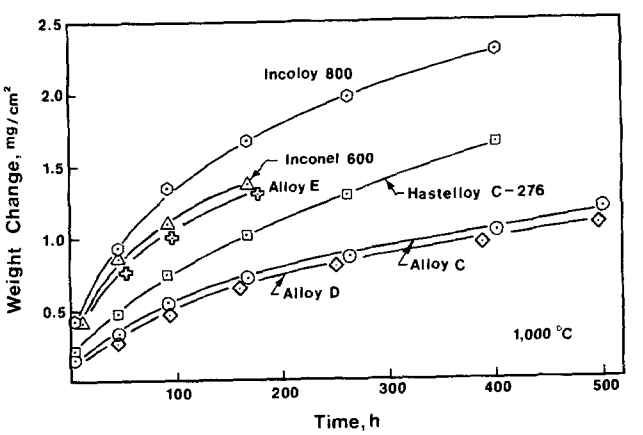

Fig. 4. Reaction kinetics of alloys C, D, and E compared to some commercial superalloys at 1000°C.

ception of alloy A, the weight changes of these alloys were so small they were hardly detectable. Alloy A showed a weight gain of 0.81 mg/cm^2 after 24h of oxidation. Therefore, alloys B, C, D, and E were oxidized for 1000h at 600°C with a single thermal cycle to room temperature. These specimens were removed from the furnace, weighed, and replaced in the furnace after 500h of oxidation. Even after 1000h of oxidation, almost negligible weight gains were observed.

Figure 1 illustrates the thermogravimetric data for the alloys at 750°C. Data for 304 SS and pure iron are included for comparison. Alloys B, C, D, and E show almost identical weight gains, so only alloy C is depicted. These alloys show excellent oxidation resistance at 750°C, having weight changes only slightly over the accuracy limits of the balance. Again, these alloys were oxidized for 1000h with multiple (ten times) thermal cyclings, however, almost no further weight changes were observed.

Table II. Parabolic oxidation rate constants

Alloy	900°C	950°C (mg^2/cm^4/s)
C	2.1×10^{-8}	1.7×10^{-7}
D	1.9×10^{-8}	—
E	4.3×10^{-7}	9.0×10^{-7}

These alloys were oxidized for 40h at 900°C with a thermal cycling after 20h of oxidation. Again, alloys B, C, and D show small weight gains. Alloy E shows a somewhat higher oxidation rate than the others, but it still performs

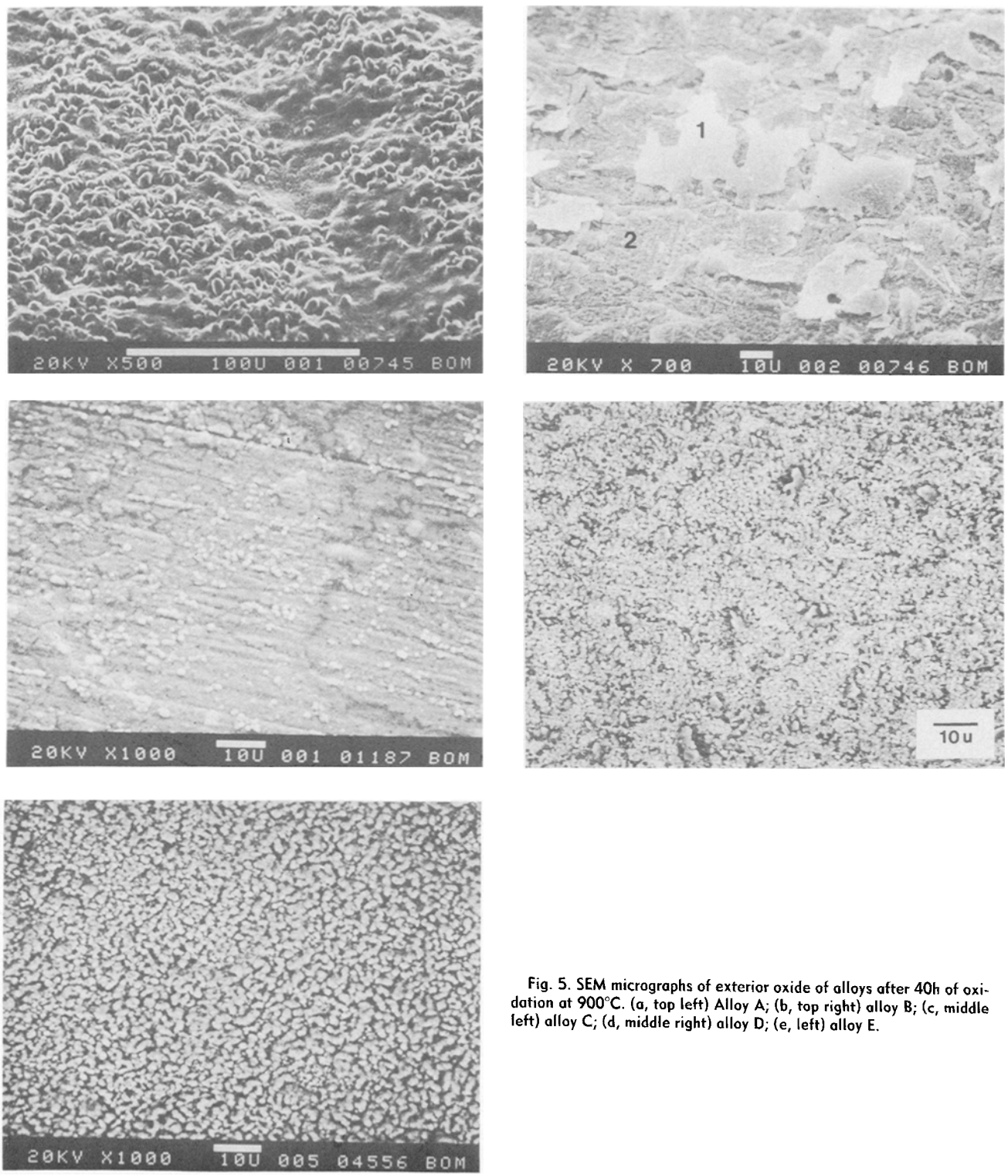

Fig. 5. SEM micrographs of exterior oxide of alloys after 40h of oxidation at 900°C. (a, top left) Alloy A; (b, top right) alloy B; (c, middle left) alloy C; (d, middle right) alloy D; (e, left) alloy E.

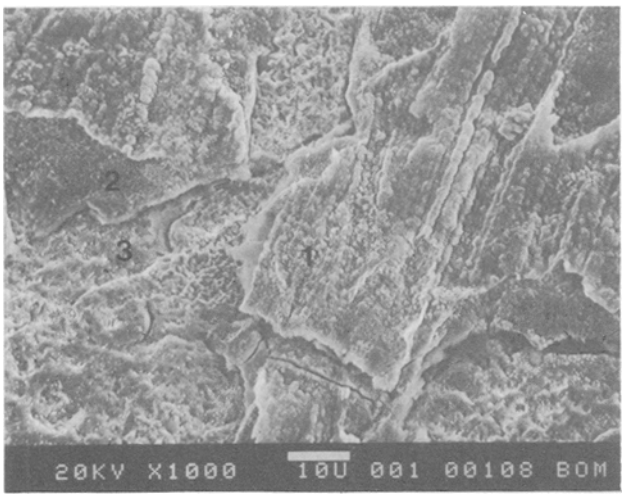

Fig. 6. SEM micrographs of exterior oxide of alloy D after 20h of oxidation at 1000°C.

better than 304 SS. These results indicate that a small addition of manganese increases the oxidation rate at high temperatures. Most of these alloys were not significantly affected by thermal cycling. Alloys B, C, D, and E were oxidized for 500h at 900°C with several thermal cyclings (1, 3, 10, 30, 100, 300, and 500h) as shown in Fig. 2. Again, 304 SS is included for comparison. No breakaway oxidation was observed. Alloy B showed microspalling during thermal cycling. Most alloys oxidized at rates in accordance with a parabolic rate law.

Alloys C, D, and E were oxidized by thermal cycling for 1000h at 950°C as shown in Fig. 3. Each data point represents the weight change after each thermal cycle. Generally, alloys obeyed a parabolic rate law, except alloy D, which showed less weight gain at an early stage of oxidation. Alloy E showed about three times higher oxidation rate than alloys C and D. The parabolic rate constants of alloys at 900° and 950°C are presented in Table II.

Since the oxidation resistance of these alloys was good, the alloys were compared with some commercial superalloys as shown in Fig. 4. The alloys were oxidized for 500h at 1000°C with thermal cyclings at 8, 40, 90, 175, 275, 400, and 500h. Surprisingly, alloys C and D outperformed the commercial superalloys. Alloy E and Inconel 600 showed similar reaction kinetics and also spalled at the same time after several thermal cyclings. Incoloy 800 and Hastelloy C-276 also spalled after 400h of oxidation.

Morphology and composition of oxide and base metal.— The morphology and composition of the oxide scale and base metal were examined by optical microscopy, SEM, EDXA, and x-ray diffraction. The oxide scales that formed at 600° and 750°C for all alloys except alloy A were so thin they were difficult to analyze. Oxidation had barely tarnished their bright metallic finish. Alloys D and E showed some degree of metallic shine even after 1000h of oxidation. Under SEM observation, an extremely thin oxide was observed on the surface of these specimens.

At 900°C, the alloys formed different oxide morphologies after 40h of oxidation, as shown in Fig. 5. Note that small amounts of alloying elements contribute to a change in the morphology of the oxides. Alloy A formed a thick iron oxide, while alloy B formed a thin protective layer. This observation indicates that the addition of silicon completely suppressed the formation of iron oxide. The EDXA analyses were conducted at areas 1 and 2 in alloy B (Fig. 5b). Area 1 was rich in Cr, while area 2 showed a similar composition to that of the base metal. Alloy E was mounted in epoxy and then cross-sectioned to obtain a concentration profile of the elements. The oxide showed

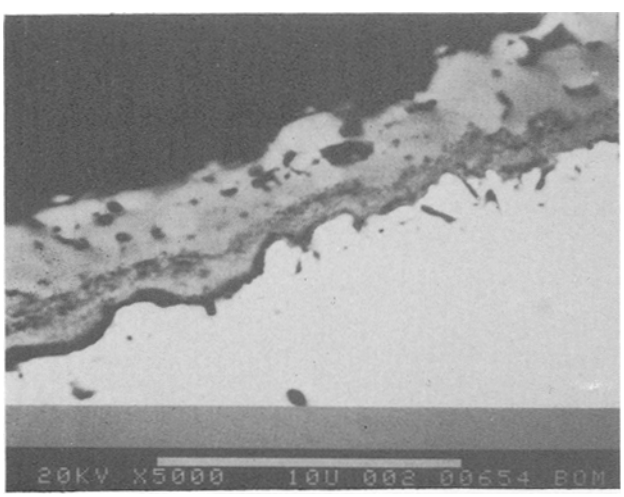

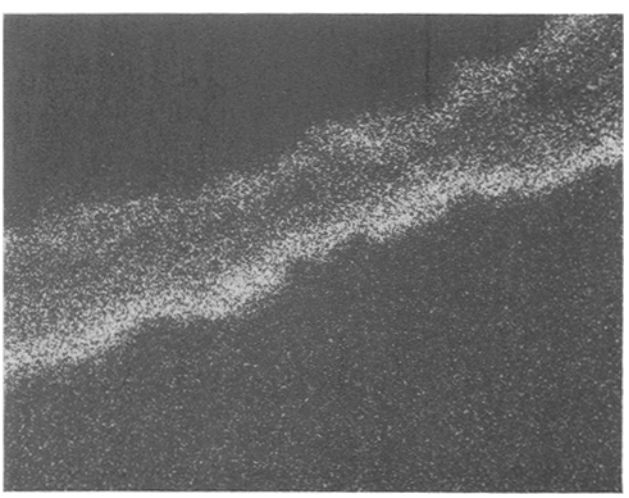

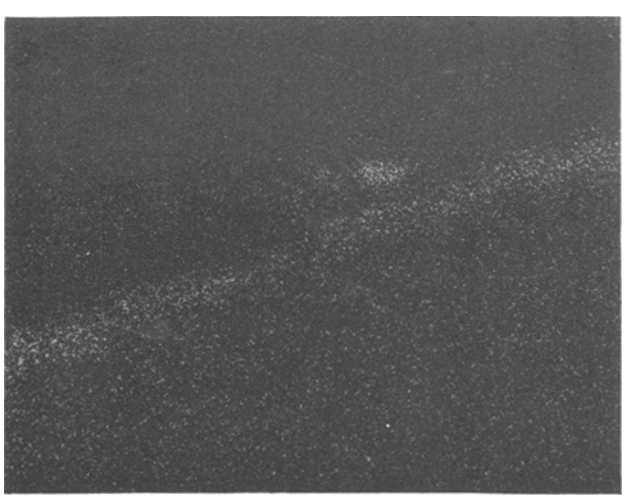

Fig. 7. SEM and EDXA micrographs of a sample of alloy C which was cross-sectioned after 100h of oxidation at 1000°C. (a, top left) Cross-sectional view; (b, above) Cr x-ray map; (c, left) Si x-ray map.

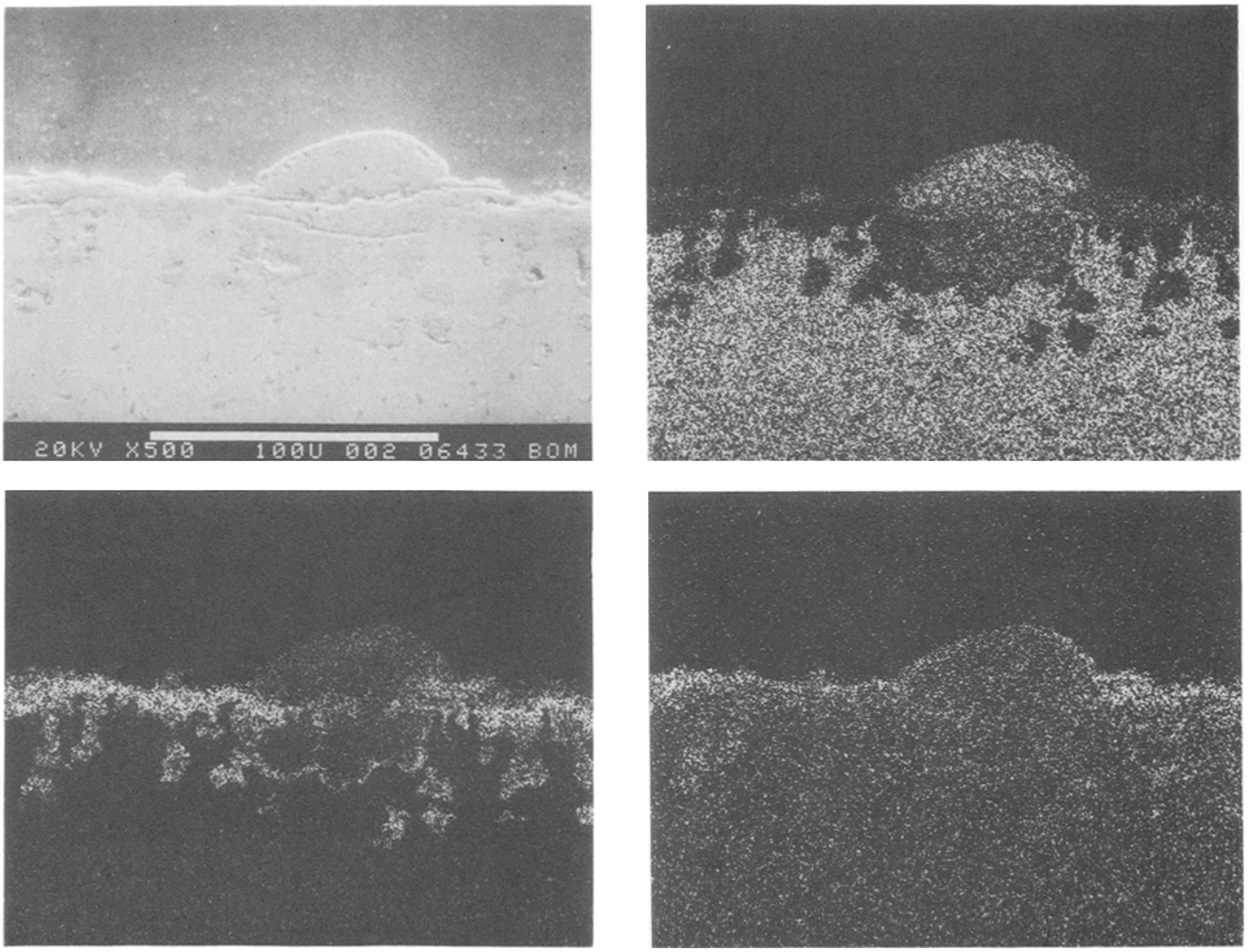

Fig. 8. SEM and EDXA micrographs of a sample of alloy E which was cross-sectioned after 250h of oxidation at 1000°C. (a, top left) Cross-sectional view; (b, top right) Cr x-ray map; (c, bottom left) Fe x-ray map; (d, bottom right) Mn x-ray map.

an enrichment of Mn in the outermost layer, and Cr was the main element in the oxide. Also, some aluminum was concentrated at the scale-metal interface.

Since the oxides forming on these alloys were not thick enough to separate them from the base metal, x-ray diffraction was performed directly on the specimen surface. The data are summarized in Table III.

At 1000°C, the alloys formed thicker oxides, which were easier to analyze. The surface morphology of the oxides was similar to that at 900°C except the oxides had grown bigger. Again, the flake-like oxides in alloy B were rich in Cr. A high concentration of Mn was observed in alloy E by EDXA analysis. Alloy D showed three different oxide layers had developed during 20h of oxidation as shown in Fig. 6. The EDXA analyses for different oxide layers were tabulated in Table IV. Alloy C was oxidized for 100h, and then cross-sectioned as shown in Fig. 7. The oxide was rich in Cr, while Si was uniformly concentrated at the scale-metal interface. After longer exposure, well-developed chromium oxide is the main oxide to form a dense, protective layer. Figure 8 shows the cross-sectional view of alloy E with elemental x-ray maps after 250h of oxidation. The oxide penetrated deeply into the base metal, and iron oxide started to form. Manganese was concentrated at the outermost layer.

Table III. X-ray diffraction results (40h at 900°C)

Alloy	Oxide composition
A	Fe_2O_3 (M), $FeCr_2O_4$ (t), FeO (t)
B	Cr_2O_3 (M), Fe_2O_3 (t)
C	Cr_2O_3 (M), Al_2O_3 (m)
D	Cr_2O_3 (M), Al_2O_3 (m)
E	Cr_2O_3 (M), $(Cr,Mn)_3O_4$ (m), $(Fe,Cr)_2O_3$ (t)

M, major; m, minor, t, trace.

Table IV. EDXA analyses for oxide formed on alloy D (weight percent)

Element	Fe	Ni	Cr	Si	Al
Area 1	22.37	19.55	46.42	1.16	10.5
Area 2	25.38	28.8	41.8	1.23	2.78
Area 3	18.5	2.67	76.26	0.98	1.6

Discussion

To develop low chromium substitute alloys, several factors were considered. First of all, the substitution was aimed at 304 SS because it consumes the largest quantity of chromium of any metal alloy in the United States. Therefore, lowering the chromium content, yet maintaining the oxidation resistance and the austenitic structure, was the important consideration.

Alloys A, B, and C contain martensite after cooling to room temperature. The addition of molybdenum yields two advantages: (*i*) solution hardening and (*ii*) lowering the martensite start temperature, hence stabilizing the austenite. Consequently, alloy D exhibits an austenitic microstructure. However, edge cracking was experienced during hot working because the molybdenum decreases the ductility during hot working (7). This problem was resolved by adding a small amount of manganese, which is a common minor element in stainless steels and also helps to stabilize the austenitic microstructure. Alloy E, containing both Mo and Mn, has an austenitic structure and did not crack during hot working.

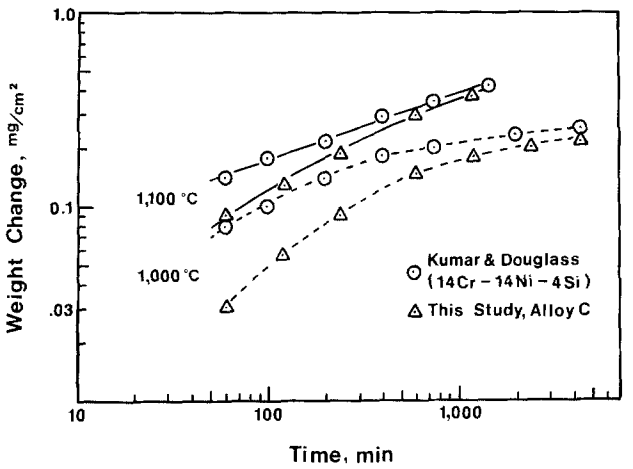

Fig. 9. Comparison of the reaction kinetics of alloy C with previous data.

The thermogravimetric data and morphology of oxide are consistent at 600° and 750°C. Extremely small weight changes were observed, along with extremely thin oxide formation. Consequently, great difficulty was experienced in analyzing the oxidation products of all the alloys except alloy A. Alloy A contained 8% chromium, which is obviously too low to form a protective layer. The addition of silicon completely changed the oxidation behavior. Silicon acted like a secondary oxygen getter to help the formation of chromium oxide. The important role of silicon in oxidation will be discussed later.

At higher temperatures, the effects of the alloying elements on the oxidation rate and morphology are noticeable. Alloy B formed a flake like oxide because of the microspalling during thermal cycling. Although the microspalling occurred, no breakaway oxidation was observed during many thermal cycles at 900°C. It is apparent from these results that silicon plays the important role of protecting the underlying metal. The effect of silicon on oxidation resistance has been known for many years (8-18). Particularly, the effect of silicon on increased oxidation protection for 304 SS was investigated by many authors (16, 17, 19). If the silicon content is high enough, a continuous silica or silicate layer forms at the scale-metal interface to provide good oxidation resistance. However, if the Si content is too high, it will impart brittleness to the alloy, or may decrease the useful life by increasing the alloy's secondary creep rate. High silicon also may form a low melting fayalite during steel making that causes problems (15, 20). This research shows that 3-3.5% Si, with proper Cr and Al additions, provides effective oxidation resistance.

When a small amount of Al was added (alloy C), no spalling was observed and Cr oxides were more conglomerated. The additions of aluminum also play an important role in improving the oxidation resistance. For example, Kumar and Douglass investigated a modified alloy containing 14% Cr with Si additions. The oxidation of this alloy is compared to that of alloy C, as shown in Fig. 9. Alloy C clearly shows a lower oxidation rate with a lower chromium content than Kumar's modified alloy during the transient and overall oxidation period. For a better understanding of the oxidation processes at higher temperatures, samples of alloy C were oxidized at 1000°C for 24 and 120h. To observe the oxide-metal interface, the underlying base metal was removed by a bromine-alcohol solution.

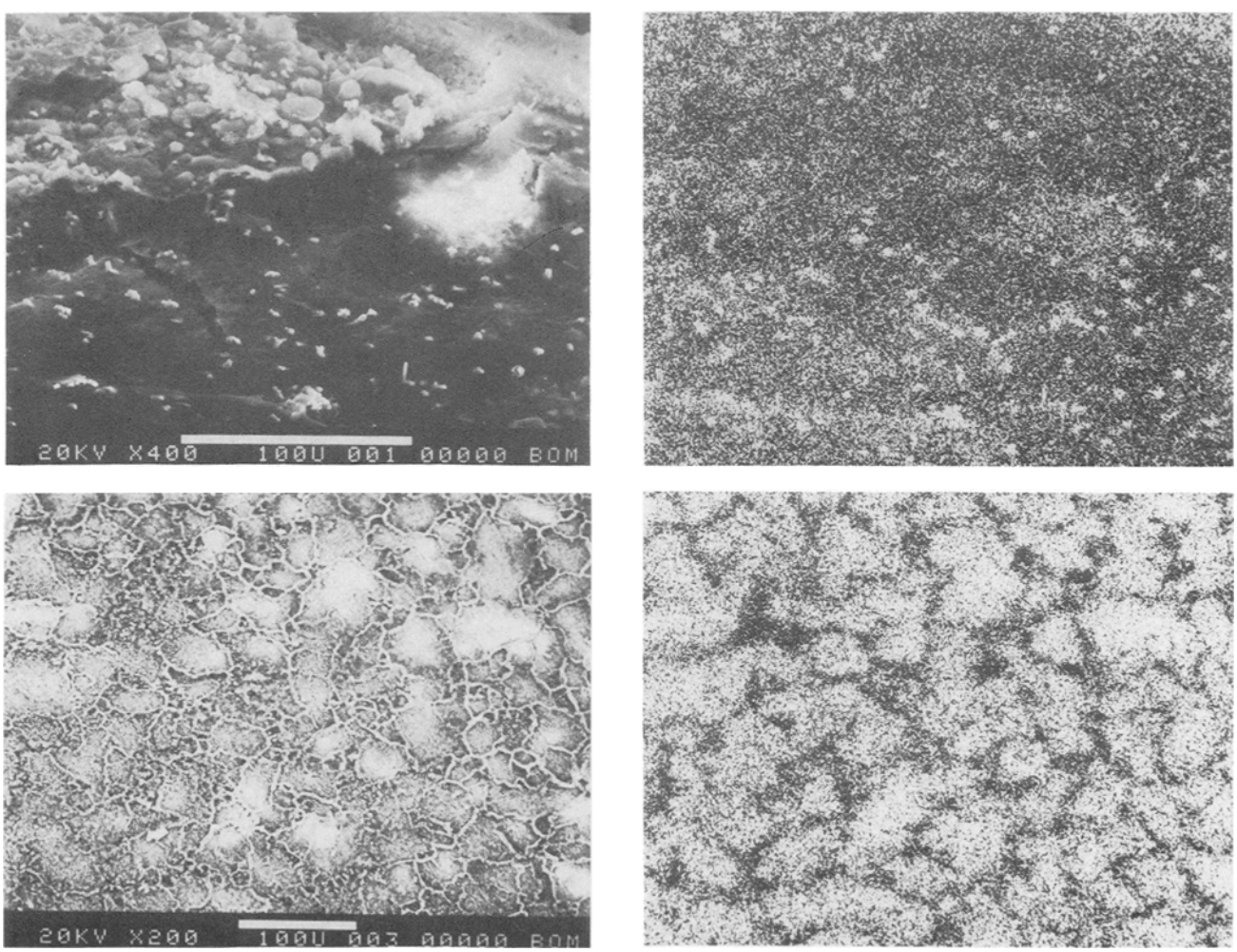

Fig. 10. SEM micrographs of the bottom of the oxide from alloy C (a, top left) after 24h of oxidation at 1000°C; (b, top right) Al x-ray map; (c, bottom left) after 120h of oxidation at 1000°C; (d, bottom right) Cr x-ray map. Specimens prepared by removing base metal with bromine-alcohol solution.

Figure 10 shows the bottom of the oxides and x-ray maps of Al and Cr. The aluminum oxides apparently nucleate at grain boundaries and then peg into the grain boundaries so that the oxide adherence is improved. This also may help an Si layer and/or Cr oxide to form more effectively. After longer exposures, the Al and Si were more concentrated at the grain boundaries, which resulted in a higher concentration of Cr within the grains, as shown in Fig. 11b. It appears that aluminum increases oxide adherence and also decreases the transient oxidation rate. It may be possible to form a mullite, which is the most thermodynamically stable oxide in these temperature ranges; however, no mullite was observed by x-ray diffraction.

Molybdenum is known to cause catastrophic oxidation of Fe-Cr-Mo alloys in some concentration ranges (21). No catastrophic oxidation occurred in these alloys, possibly because of the low concentration of Cr and Mo. Molybdenum had the beneficial effect of promoting the formation of an external protective Al_2O_3 layer during oxidation of rapidly solidified Ni-Al-Mo alloys (22). Molybdenum has been shown to form an Fe-Mo silicide at the grain boundaries to reduce oxidation (23). Additions of 2% molybdenum to alloys D and E had effects on their oxidation. These two alloys showed more metallic shine after 1000h of oxidation at 600° and 750°C, and slightly lower oxidation rates were observed at 950° and 1000°C than those of alloys B and C. Also, alloy D had more expanded chromium oxide coverage than alloy C, as shown in Fig. 5. It appears that Mo decreases the formation of transient oxides by promoting the rapid formation of Cr oxides.

The addition of Mn in the base metal increases the oxidation rate because manganese is the fastest diffusing element in this alloy.

Summary and Conclusion

From the foregoing data, the improved oxidation resistance of alloys B, C, D, and E compared with alloy A shows that Si plays an important role as a secondary oxygen getter to help in the formation of Cr oxide. As mentioned earlier, 8% Cr is not enough to form a protective chromia layer. However, the synergistic effect of Al, Cr, and Si promotes a good oxidation resistance in these alloys containing low Cr. The silicon containing layer which was formed at the scale-metal interface was very effective in controlling the oxidation process. Small additions of aluminum also are needed to reduce transient oxidation and to increase oxide adherence. Thermodynamically stable oxide formers, such as Al and Si, compensate for the deficiency of Cr in these low Cr alloys.

All of these alloys except alloy A show much better oxidation resistance than 304 SS. However, only alloy E has an austenite microstructure at room temperature with no difficulty during hot working. Therefore, alloy E may be a suitable substitute for 304 SS. With slight compositional modifications, alloys C and D can be used for higher temperature applications than existing stainless steels. Superior oxidation resistance of alloys C and D, over some commercial superalloys, is very impressive. Therefore, lower chromium substitute alloys can be developed with suitable additions of some minor alloying elements.

Acknowledgment

The author would like to thank Professor M. J. McNallan, University of Illinois at Chicago, for his useful discussions.

Manuscript submitted March 20, 1987; revised manuscript received Aug. 26, 1987.

Albany Research Center assisted in meeting the publication costs of this article.

REFERENCES

1. J. Garcia, N. Rosas, and R. Rioja, *Met. Prog.*, **122,** 47 (1982).
2. J. Dunning, *U.S. Bur. Mines, Rep. Invest.* 8856 (1984).
3. R.Wang, M. Straszheim, and R. Rapp, *Oxid. Met.*, **21,** 71 (1984).
4. J. Oh, M. McNallan, and W. King, *This Journal,* **133,** 1042 (1986).
5. J. Stephens and C. Barret, *NASA Techn. Rep.*, **6,** 1557 (1979).
6. S. Floreen, *Metall. Trans.*, **13A,** 2003 (1982).
7. D. Pecker and I. Bernstein, "Handbook of Stainless Steel," Chap. 13-10, McGraw Hill, Inc., New York (1977).
8. J. Evans and S. Chatterji, *This Journal,* **106,** 860 (1959).
9. G. C. Wood, J. A. Richardson, M. G. Hobby, and J. Boustead, *Corros. Sci.*, **9,** 659 (1970).
10. D. Douglass and J. Armijo, *Oxid. Met.*, **2,** (2), 207 (1970).
11. F. H. Fern and J. E. Antill, *Corros. Sci.*, **10,** 649 (1970).
12. C. E. Lowell, *Oxid. Met.*, **10,** 1 (1973).
13. I. Svedung and N. Vannerberg, *Corros. Sci.*, **14,** 391 (1974).
14. D. Jones and J. Stringer, *Oxid. Met.*, **9,** (5), 409 (1975).
15. A. Kumar and D. Douglass, *ibid.*, **10,** (1), 1 (1976).
16. M. D. Merz, *Metall. Trans. A,* **10,** 71 (1979).
17. G. Yurek, D. Eisen, and A. Garratt-Reed, *ibid.*, **13,** 473 (1982).
18. H. Evans, D. Hilton, R. Holm, and S. Webster, *Oxid. Met.*, **19,** (1/2), 1 (1983).
19. M. Landkof, A. V. Levy, D. H. Boone, R. Gray, and E. Yaniv, *Corrosion (Houston),* (6), 344 (1985).
20. W. Boggs, *Oxid. Met.*, **10,** (4), 277 (1976).
21. S. Brenner, *This Journal,* **102,** 16 (1955).
22. G. Meier, F. Pettit, and A. Khan, in "Proceedings of Third Conference on Rapid Solidification," NBS, 348, Washington, DC (1982).
23. J. Rawers, *Mat. Sci. Lett.*, 513 (May 1986).